

Search for transitions between states in redbacks and black widows using seven years of *Fermi*-LAT observations

Diego F. Torres^{1,2}, Long Ji^{3,4}, Jian Li¹, Alessandro Papitto⁵
Nanda Rea^{1,6}, Emma de Oña Wilhelmi¹, Shu Zhang³

ABSTRACT

Considering about seven years of *Fermi*-Large Area Telescope (LAT) data, we present a systematic search for variability possibly related to transitions between states in redbacks and black widow systems. Transitions are characterized by sudden and significant changes in the gamma-ray flux that persist on a timescale much larger than the orbital period. This phenomenology was already detected in the case of two redback systems, PSR J1023+0038 and PSR J1227–4853, for which we present here a dedicated study. We show the existence of only one transition for each of these systems over the past seven years. We determine their spectra, establishing high-energy cutoffs at a few GeV for the high gamma-ray state of PSR J1023+0038 and for both states of PSR J1227–4853. The surveying capability of the *Fermi*-LAT allows studying whether similar phenomenology has occurred in other sources. Although we have not found any hint for a state transition for most of the studied pulsars, we note two black-widow systems, PSR J2234+0944 and PSR J1446–4701, whose apparent variability is reminiscent of the transitions in PSR J1023+0038 and PSR J1227–4853. For the other systems we set limits on potential transitions in their measured gamma-ray light curves.

Subject headings: gamma-ray: observations, pulsars: individual (PSR J1023+0038, PSR J1227–4853)

¹Institute of Space Sciences (IEEC-CSIC), Campus UAB, Carrer de Magrans s/n, 08193 Barcelona, Spain

²Institució Catalana de Recerca i Estudis Avançats (ICREA), E-08010 Barcelona, Spain

³Key Laboratory for Particle Astrophysics, Institute of High Energy Physics, Chinese Academy of Sciences, 19B Yuquan Road, Beijing 100049, China

⁴Institut für Astronomie und Astrophysik, Kepler Center for Astro and Particle Physics, Sand 1, D-72076 Tübingen, Germany

⁵INAF-Osservatorio Astronomico di Roma, via di Frascati 33, I-00040 Monte Porzio Catone, Roma, Italy

⁶Anton Pannekoek Institute, University of Amsterdam, Postbus 94249, NL-1090-GE Amsterdam, The Netherlands

1. Introduction

In the framework of the recycling pulsar model, the rapid spinning of old millisecond pulsars is the outcome of accretion of mass transferred by a low-mass late-type companion star onto a neutron star (NS) via an accretion disk (Alpar et al. 1982). After a Gyr-long mass accretion phase during which the binary system shines as a bright low mass X-ray binary (NS-LMXB), the mass transfer rate declines and allows the activation of a radio/gamma-ray millisecond pulsar (MSP) powered by the rotation of its magnetic field.

The tight link existing between radio MSPs and NS-LMXBs has been only recently demonstrated by the discovery of three transitional millisecond pulsars (PSR J1023+0038, Archibald et al. 2009; PSR J1824–2452I in the globular cluster M28, Papitto et al. 2013; and XSS J12270–4859 / PSR J1227–4853, de Martino et al. 2010, 2013, 2015, Bassa et al. 2014).

These sources have been observed to switch between accretion and rotation-powered emission on timescales possibly shorter than a couple of weeks. Thus, such state transitions may take place on timescales compatible with those of the variations of the mass accretion rate onto the NS.

Under this hypothesis (see e.g., Bogdanov 2015 and other references above), at high mass inflow rates, the radio pulsar is shut-off and the system is bright in X-rays ($L_X > 10^{36}$ erg s⁻¹). At low mass inflow rates, the magnetosphere probably expands up to the light cylinder, activating the radio pulsar; the disk disappears and the system is instead quiet in X-rays ($L_X \sim 10^{32}$ erg/s).

In addition to the accreting and the radio pulsar states, the transitional pulsars known so far have been observed to enter into a sub-luminous disk state with $L_X \sim 10^{33}$ erg/s. During this state, both J1023+0038 (Archibald et al. 2015; in the text below we will omit the “PSR” or “3FGL” prefix of the sources for simplicity) and J1227–4853 (Papitto et al. 2015) have 6–8% of the X-ray flux pulsed. Most likely, then, a part of the disk material is accreted onto the NS surface. In addition, these sub-luminous states are accompanied by a sizeable gamma-ray flux and a flat radio spectrum that are typical signatures of jets in accreting compact objects, suggesting that large mass outflows could be launched by these pulsars. These features prompted theoretical models based on the propeller mechanism (Papitto, Torres, & Li 2014; Papitto & Torres 2015, Campana et. al. 2016).

Currently, the timescales of the transitions are only loosely constrained, but are of primary importance because they reflect the timescale of disk formation and the transition into a jet-dominated outflow or of the disk evaporation. Candidate transitional pulsars are identified among binary radio millisecond pulsars whose donor stars are currently losing

mass, as indicated by the irregular eclipses of the radio pulsed emission caused by absorption and scattering by the matter ejected from the system. They are tight binaries ($P_{orb} < 1$ day), and are dubbed black widows (BWs, $M_{companion} \ll 0.1 M_{sun}$; Fruchter et al. 1988) or redbacks (RBs, $M_{companion} \sim 0.2 - 0.4 M_{sun}$; D’Amico et al. 2001), depending on the mass of the companion. Tens of systems of this kind were discovered by radio surveys in our Galaxy (see the ATNF Pulsar Catalog¹, Manchester et al. 2015). They possess a similar spin distribution, which is intermediate between the faster accretion-powered millisecond pulsars and the slower non-eclipsing rotation-powered millisecond pulsars, and are evolutionarily linked (Chen et al. 2013, Papitto et al. 2014).

Here we analyze *Fermi*-LAT data to systematically search for transitions, not only in the known transitional pulsars, but in a large sample of RBs and BWs.

2. Observations and data analysis

The *Fermi*-LAT data included in this report cover nearly seven years, from 2008 August 4 (MJD 54682) to 2015 June 1 (MJD 57198). The analysis of *Fermi*-LAT data was performed using the *Fermi* Science Tools 10-00-05 release². Events from the “Pass 8” event class were selected. The “Pass 8 R2 v6 Source” instrument response functions (IRFs) were used in the analysis. We have considered all gamma-ray photons within the energy range 0.1–300 GeV for circular regions of interest (ROI) of 10° radius around each of the RBs & BWs. Additionally, to reject contaminating gamma rays from the Earth’s limb, we have only selected events with zenith angle $< 90^\circ$. The systematic errors have been estimated by repeating the analysis using modified IRFs that bracket the effective area (Ackermann et al. 2012), and artificially changing the normalization of the Galactic diffuse emission model by $\pm 6\%$ (Abdo et al. 2013). However, note that changes of measured fluxes evaluated with and without systematic uncertainties considered are far lower than the flux jumps we are seeking here, i.e., usually few percent compared to a jump in flux by a factor of several.

The gamma-ray fluxes presented in this work were calculated by performing a binned maximum likelihood fit using the Science Tool *gtlike*. The spectral-spatial model constructed to perform the likelihood analysis includes Galactic and isotropic diffuse emission components (“gll_iem_v06.fits”, Acero et al. 2016, and “iso_P8R2_SOURCE_V6_v06.txt”, respectively³),

¹<http://www.atnf.csiro.au/people/pulsar/psrcat/>

²<http://fermi.gsfc.nasa.gov/ssc/>

³<http://fermi.gsfc.nasa.gov/ssc/data/access/lat/BackgroundModels.html>

as well as known gamma-ray sources within 15° of the source analyzed, as included in the third *Fermi* Source Catalog (Acero et al. 2015, 3FGL hereafter). The spectral parameters and the positions of all gamma-ray sources were fixed to the catalog values, except for those within 3° from the considered targets. For these latter sources, the spectral parameters were left free. In the cases of previously known associations between gamma-ray sources and RBs or BWs (see Table 1), we have adopted the spectral shape reported in the 3FGL. If no association was made earlier, their spectra were modelled with a simple power law. All spectral parameters of RBs and BWs were allowed to vary.

The test statistic (TS, Mattox et al. 1996) was employed to evaluate the significance of the gamma-ray fluxes from the sources. The TS is defined by $TS = -2 \ln(L_{max,0}/L_{max,1})$, where $L_{max,0}$ is the maximum likelihood value for a model without an additional source (the “null hypothesis”) and $L_{max,1}$ is the maximum likelihood value for a model with the additional source at a specified location. A larger TS indicates that the null hypothesis is not preferred. The TS is distributed as χ^2 so that a gamma-ray excess at the tested position can be deemed significant if $TS > 25$.

3. Search for state transitions in long-term light curves

We have carried out the analysis of the 12 confirmed RBs and the 18 confirmed BWs (Table 1). The transitional millisecond pulsar PSR J1824–2452I is not included in the analysis, since it is located in the globular cluster M28, which is a bright gamma-ray source (Abdo et al. 2010a). To search for possible state transitions in RBs and BWs, we produced long-term light curves for all systems in Table 1. The average TS values, spectral parameters, and average fluxes along the whole observation period for all systems in our search are shown in Table 1.

RBs and BWs usually host gamma-ray pulsars. Eleven out of 12 RBs, and 15 out of the 18 BWs are significantly detected in the 0.1–300 GeV band. In the second *Fermi* Large Area Telescope Catalog of Gamma-Ray Pulsars (Abdo et al. 2013, 2PC hereafter), pulsations in gamma rays were identified in one out of four RBs known at that time, and 10 out of 16 BWs known at that time. With more *Fermi*-LAT data accumulated (seven years against the three years considered in the 2PC), the use of a more advanced event-level analysis (Pass 8 against Pass 7), and a better modelling of the gamma-ray sky (3FGL against 2FGL), more gamma-ray pulsars were found in known RBs and BWs by the *Fermi*-LAT collaboration⁴

⁴<https://confluence.slac.stanford.edu/display/GLAMCOG/Public+List+of+LAT-Detected+Gamma-Ray+Pulsars>, noted as “list” in Table 1.

(Table 1). Currently, seven out of 12 RBs, and 15 out of 18 BWs are already known to pulse in gamma rays, which clearly contribute to the detected gamma-ray emission. The current non-detection of gamma-ray pulsars among the rest of the RBs and BWs may be a result of limited gamma-ray statistics, not well known pulsar ephemerides and/or binary parameters, or an unfavorable beaming direction of the pulsar gamma-ray emission with respect to our line of sight (Guillemot & Tauris 2014).

Using distances from the radio dispersion measure when available⁵(Cordes & Lazio 2002), we converted the gamma-ray fluxes into corresponding luminosities (L_γ), which are also listed in Table 1. The gamma-ray luminosities ($L_\gamma = 4\pi D^2 F$, D and F are the distance and flux in Table 1) of RBs and BWs range from $\sim 10^{33}$ erg s⁻¹ to $\sim 10^{35}$ erg s⁻¹.

During the state transitions of the few transitional millisecond pulsars known (i.e., in the cases of J1023+0038, Stappers et al. 2014; and J1227–4853, Johnson et al. 2015; both being RB systems) their gamma-ray flux was observed to vary by a factor of 2 to 5.

3.1. A fixed time binning and analysis of the known transitional pulsars

We initially used a time bin of 60 days to construct the light curves (Fig. 1). This was the timescale earlier used to analyze and discover the known transitional pulsars (see, e.g., Stappers et al. 2014, Bogdanov & Halpern 2015, also Bogdanov 2016). It is also a sensible time bin selection for the average fluxes presented here; if the time bin is significantly shorter than this timescale, there would be too few counts per bin in many cases; if it is significantly larger than this timescale, there would be fewer bins to search for the light curve evolution and transitions of duration of up to several months could be missed. Below we also explore other timescales chosen on a case-by-case basis. Flux upper limits (95% confidence level) were calculated using Helene’s method (Helene 1983), assuming the photon index in Table 1 if the TS value of a time bin is below 12 ($\sim 3.5\sigma$, dotted green line in Fig. 1).

Significant flux variations are found in this analysis only in the cases of J1023+0038 and J1227–4853, at the already known state transitions times (see Fig. 1, where the dotted vertical line indicates the time at which they happen). These results are in agreement with those of Stappers et al. (2014) for J1023+0038 and Xing & Wang (2015) for J1227–4853. Note that the transitions in J1023+0038 and J1227–4853 occur in opposite directions; i.e., while for J1023+0038 the transition is from a radio pulsar state (low gamma-ray state) to a sub-luminous disk state (high gamma-ray state), it is the opposite for J1227–4853. Assuming

⁵<http://www.atnf.csiro.au/research/pulsar/psrcat/>

the same physical mechanism is at work in both sources, the back and forth nature of the swinging phenomenon is emphasized by this fact. No other transition at earlier or later times is discovered in the additional dataset analyzed here.

We modelled J1023+0038 and J1227–4853 while being in radio pulsar and sub-luminous disk states using a power-law function with and without an exponential cutoff. A spectral cutoff at $E_{cut}=3.7 \pm 1.3 \pm 0.9$ GeV (as usual the first error comes from statistics and the second from systematics) was detected for J1023+0038 in the sub-luminous disk state, with a spectral index of $2.0 \pm 0.1 \pm 0.1$. The likelihood ratio test indicates a Δ TS of 18.9, which indicates that the significance of the spectral cutoff is $\sim 4.3\sigma$. No spectral cutoff is detected for J1023+0038 during its radio pulsar state, which is consistent with the reports by Takata et al. (2014) and Tam et al. (2010). The SEDs of J1023+0038 during radio pulsar state and sub-luminous disk state are shown in Fig. 2.

Spectral cutoffs are hinted at for J1227–4853 during both periods, before and after the gamma-ray transition. Before the transition, in the sub-luminous disk state of the source, a spectral cutoff at $E_{cut}=10.8 \pm 3.7 \pm 5.6$ GeV, with a power-law having a spectral index of $2.3 \pm 0.1 \pm 0.1$, yields a Δ TS of 13.9 (which implies it is a better fit than a simple power-law at $\sim 3.7\sigma$). After the transition, in the radio pulsar state of the source, the existence of a cutoff provides a Δ TS of 11.4 ($\sim 3.4\sigma$), so that J1227–4853 is better described by a power law with cutoff at $E_{cut}=5.3 \pm 2.5 \pm 2.3$ GeV and spectral index of $2.0 \pm 0.1 \pm 0.3$. The cutoff energies and spectral indices before and after the transition are compatible within their corresponding 1σ errors, and are consistent with the values reported by Johnson et al. (2015) and Xing & Wang (2015).

3.2. A flux-motivated definition of the time binning

Using the fitted model from the approximately seven years binned maximum likelihood analysis and the tool *gtobssim*, we produced simulated *Fermi*-LAT observational data for each of the sources of interest. Simulated data were produced for different exposure times, in a similar region of interest to the real data, and were analyzed following the standard steps described in Section 2. The simulated TS values of RBs and BWs were obtained for the different exposure times assigned in the simulation, and were fitted by a linear function. With the fitted linear function, we estimated the observation time needed for a TS=25-detection with the *Fermi*-LAT at 90% confidence level for the average level of flux given in Table 1. This estimation gives a natural time binning for each source that is adequate for the corresponding level of flux: under the assumption of no variability, the extent of each time bin should be enough to result in a detection of the source with a TS value around 25.

With the time binning so defined for each source, we produced the corresponding long-term light curves.

To each of these light curves, we fitted a constant and computed the χ^2 , as described in Abdo et al. (2010b). Table 2 gives for each source the results of this fitting, and the time bin used for each source. In particular, the P -value (probability of the flux being constant) and the corresponding σ indicate the significance of flux variability. We see that the obtained light curves are all compatible with no persistent jump in flux (no transition) except for the known transitional pulsars and two other cases.

The case of the transitions in J1023+0038 and J1227–4853 is shown in Fig. 3 (upper panels). For the former, applying the simulation-determined binning of 9 days results in a number of upper limits before the transition and a number of significant detections just after; the transition is obvious. The smaller variation of flux between the high and the low gamma-ray state of J1227–4853 allows for significant detections before and after the transition. The bin width resulting from the simulations is in this case larger (53 days). Table 2 shows that for J1227–4853, the hypothesis of constant flux is rejected with $\sim 10 \sigma$ confidence. In the low state, the flux evolution is compatible with a constant. However, in the high gamma-ray state of J1227–4853, a constant flux is put in question (ruled out with a significance of 4.7σ), likely indicating the action of shorter-timescale phenomena.

The variability appearing in J1446–4701 and J2234+0944 seems reminiscent of the phenomenology shown by J1023+0038 and J1227–4853, despite the caveat (especially for J1446–4701) of their lower fluxes. Their light curves are shown in Fig. 3 (lower panels). A constant line fitting is ruled out at 4.2σ and 5.5σ , respectively.

The case of J1446–4701 is difficult to assess due to its low flux. This is translated into the large time binning (506 days) needed to achieve an individually significant detection at its average flux level. With the difference between the putative *low* and *high* gamma-ray states (about a factor of 2), a firm conclusion cannot be drawn because of the lack of consecutive data points at the *high state*.

The phenomenology of J2234+0944 in gamma rays is clearer, since the greater average flux allows for a detection in a time bin of 106 days, a factor of ~ 5 shorter than that needed for J1446–4701. Given that this timescale is larger than 60 days, the possible variation of J2234+0944 was not hinted at in the fixed time bin study of the earlier section: The shorter timescale leads to larger error bars, which hide the possible flux variation. The J2234+0944 light curve shown in Fig. 3 resembles that of J1227–4853 (see second panel of Fig. 2). With constant flux being excluded (at 5.5σ), two horizontal lines separated around MJD 55500 (2010 October 31) provide correspondingly good fits: the source seems to have jumped to

a higher level of gamma-ray flux (a factor of ~ 2 higher) then. Interestingly, we note that in the two periods separated by MJD 55500, gamma-ray pulsations from J2234+0944 are significantly detected at significance greater than 8σ level, respectively. We have produced orbitally-folded light curves of J2234+0944, with an orbital period of 0.42 days (Ray et al. 2012) using all data, as well as the data before and after MJD 55500. No significant orbital modulation is detected before or after MJD 55500.

In order to assess how the variability shown in Fig. 3 could indicate a state transition we analyzed existing X-ray observations. In the period covered by *Fermi*-LAT data, there were two relatively deep X-ray observations of J1446–4701, done with *XMM-Newton* and *Swift*/XRT. The *XMM-Newton* observation was carried out on 2012 August (MJD 56140) and has 62 ks of exposure (Arumugasamy et al. 2015). The *Swift*/XRT observation was carried out in 2012 January (MJD 55932) and has 9.8 ks of exposure. However, both observations were made in the putative *low* gamma-ray state of the source. J1446–4701 was detected by *XMM-Newton* with a very low flux level of about 9×10^{-14} erg cm $^{-2}$ s $^{-1}$ in 0.5–10 keV (Arumugasamy et al. 2015). In the *Swift*/XRT observation J1446–4701 was not detected at all, yielding a compatible 95% flux upper limit in 0.5–10 keV band of about 1.2×10^{-13} erg cm $^{-2}$ s $^{-1}$, assuming a power-law spectrum with index of 2.

Two observations of J2234+0944 with *Swift*/XRT were carried out in October 2013 (MJD 56583) and April 2016 (MJD 57497); both lasted less than 6 ks. J2234+0944 was not detected in either of the observations, leading to 95% flux upper limits in 0.3–10 keV band of about 3×10^{-13} erg cm $^{-2}$ s $^{-1}$, also assuming a power-law spectrum with index of 2.

Even in the rotationally-powered state, the flux in the 0.5–10 keV range of J1227–4853 was determined to be larger than these measurements: $7.0(5) \times 10^{-13}$ erg cm $^{-2}$ s $^{-1}$ (Papitto et al. 2015). The flux from J1227–4853 in the same energy band in the high gamma-ray state is larger by more than one order of magnitude (Papitto et al. 2015). The best estimates of the distances based on the dispersion measure are 1 kpc for J2234+0944 (Ray et al. 2012) and 1.4 kpc for J1227–4853 (Roy et al. 2015). In the disk state, J1227–4853 emits an 0.5–10 keV unabsorbed flux of $\sim 2 \times 10^{-11}$ erg cm $^{-2}$ s $^{-1}$ (Papitto et al. 2015). Therefore, the upper limit on the luminosity of J2234+0944 is $\sim 5 \times 10^{-3}$ times smaller than the luminosity observed from J1227–4853. Such a low X-ray flux argues against the presence of an accretion disk for a source this close. A larger distance, however, would obviously help in making the fluxes more compatible. For instance, at a distance of ~ 3 kpc, the difference in the luminosities would be around one order of magnitude. Unless we are witnessing a transition at a much lower level of X-ray flux, a possible transition similar to that in J1227–4853 is put in doubt.

We note that the above discussion on J1446–4701 and J2234+0944 does not mean

that there is no intrinsic variability in other sources. Rather, any variability is within the errors of the fitting (i.e., within the normal evolution of the fluxes, without the appearance of a persistent jump). In particular, all sources can have transitions at shorter timescales than *Fermi*-LAT is able to test, resulting in an intrinsic flux dispersion in the time binning explored, without the appearance of an ordered transition as shown by the transitional pulsars known. In order to consider what kind of transitions *can* be detected for other sources, Table 2 shows the *jump factor*. This factor indicates the level of flux that would deviate from its mean by 3σ , assuming that the increased flux has the same uncertainty as the measured one and adding in quadrature the error of the fitted constant. Subsequently, Table 2 gives the number of data points that would be needed in the light curve at this increased flux level to be able to claim a 3σ overall variability for the light curve as a whole. Put otherwise, if we fit with a single horizontal line the whole set of points, this fitting would be ruled out with a significance larger than 3σ . We can thus quantitatively conclude that none of these transitions (nor others more significant than these) have occurred.

3.3. Conclusions

We temporally enlarged the analysis of both J1023+0038 and J1227–4853, the known transitional pulsars, by considering nearly seven years of *Fermi*-LAT data. Our results on the light curves of these systems confirmed previous reports. Only one transition is detected for each. We found that they transitioned from a low to a high state, and from a high to a low state, respectively. In addition, we determined their spectra, and confirmed the existence of high-energy cutoffs at a few GeV with the significance above 3σ for the high gamma-ray state of J1023+0038 and for both states of J1227–4853.

We searched for state transitions in all known RBs and BWs by analyzing their long term light curves in different time binnings. Our analysis included a fixed 60-day time binning, used for detection of the already known transitional pulsars mentioned above. We have also performed simulations for each source in order to determine, assuming their average level of flux, the minimum integration time needed for a *Fermi*-LAT detection at a TS=25 level. This is a flux-motivated, source-by-source-determined binning, and we have used it to study the light curves as well. By analyzing the light curves we were able to determine whether a transition has happened and if not, what are the features of the transitions that can be ruled out.

For most of the pulsars, we have not found any hint for a state transition in our search. In the light of negative results, trying to infer conclusions regarding e.g., rate of transitions, seems daunting. Transitions are inextricably linked to the local scenario, for instance, to the

variations in mass accretion rate. A negative result cannot be directly used to imply that all RBs and BWs other than the swinging ones, have actually finished any swinging phase, and are all in a final -fully recycled- state. Future surveying may prove the opposite, and when this swinging will happen, if it does, can simply not be predicted.

We found two particularly interesting cases in our search. J2234+0944 and J1446–4701 are, in contrast with the known transitional pulsars, BW systems. Both of these sources have very low companion masses. Both were discovered at Parkes as part of a radio search program for pulsars in coincidence with unidentified *Fermi*-LAT sources (see Ray et al. 2012). The radio detection of J2234+0944 was before the possible transition at MJD 55500.

J2234+0944 has a period of 3.63 ms and is part of a system with a companion of at least $0.015 M_{\odot}$, in an orbit of 0.42 days. J1446–4701 is in a system with a companion of at least $0.019 M_{\odot}$, in an orbit of 0.27 days (Keith et al. 2012). The orbits are almost circular, which is consistent with the model in which the spin-up of the pulsar is associated with Roche lobe overflow from a nearby companion. Both orbital periods are much smaller than the timescale for the variability we have found. Thus the latter can hardly have an orbital origin. But are these indeed *state transitions* similar to those found in J1023+0038 and J1227–4853?

The variability of J1446–4701 is not conclusive, although a possible back-and-forth flux jumps during the years spanned by *Fermi* observations is compatible with the data. Inconclusiveness arises from the fact of it being a very dim source in comparison to the known transitional pulsars (see Table 1), and from the (related) lack of a sufficient number of points in each of the putative states. We recommend further monitoring of this source in gamma rays and other frequencies. The variability of J2234+0944 is clearer, and a flux jump seems to have happened (see Table 2 and Fig. 3). Its brightness in gamma rays allows for a clear distinction of two states that can be deemed similar to those in J1227–4853, with an apparent transition from lower to higher gamma-ray fluxes. However, the low level of fluxes found in existing X-ray observations cast doubts that we are witnessing the same phenomenology. Future X-ray observations will tell whether this pulsar has a short timescale phenomenology as that found for J1023+0038 and J1227–4853, yet at a significantly lower level of flux. If not, we may be witnessing a gamma-ray state transition produced at the intra-binary shock and/or with a dim (if any) counterpart at lower frequencies. The latter would not be impossible within the propeller model used to investigate J1023+0038 and J1227–4853. If the propeller is strong enough to preclude any matter from reaching the surface and the disk component is significantly dimmer in X-rays in comparison with redback systems, it is in fact expected that the X-ray emission would be undetectable, smaller by even more than several orders of magnitude in comparison with that of J1023+0038 and J1227–4853 (see Fig. 1 in Papitto & Torres 2015). A proper model, together with deep

X-ray observations would help test this setting. Alternatively, we can also entertain the possibility that the pulsar magnetosphere could globally vary (see, e.g., the study by Ng et al. 2016, even though it is a very different system). If this is the case, the variation in the two states would be explained by a closer-to-the-pulsar phenomenology, and could just be interpreted as being different outer gap-generated emission, as if the pulsar would be isolated. This would naturally encompass the fact that gamma-ray pulsations are found both before and after the flux jump.

Table 1: RBs and BWs included in this report. Columns denote the source name, the 3FGL association, TS value, index, flux level, Right Ascension and Declination (J2000), whether it is detected in the 2PC/*Fermi*-LAT public pulsar catalog as of February 2016, luminosity, and distance (from the ATNF catalog). † and ‡ indicate the data period before and after the state transition for known transitional millisecond pulsars. The first/second error is statistical/systematic.

RB name	3FGL source	TS	Index	Flux (10^{-11} erg cm $^{-2}$ s $^{-1}$)	RA deg	Dec deg	2PC/list	L_γ (10^{33} ergs/s)	D (kpc)
3FGL J0523.3–2528	J0523.3–2528	1379	$2.48 \pm 0.05 \pm 0.03$	$2.03 \pm 0.11 \pm 0.06$	80.84	–25.48	no/no
PSR J1023+0038	...	1094	$2.37 \pm 0.03 \pm 0.08$	$1.96 \pm 0.01 \pm 0.13$	155.92	0.68	no/no ^a	$1.90 \pm 0.01 \pm 0.13$	0.90
PSR J1023+0038†	...	76	$2.31 \pm 0.03 \pm 0.04$	$0.50 \pm 0.09 \pm 0.05$	155.92	0.68	no/no	$0.48 \pm 0.09 \pm 0.05$	0.90
PSR J1023+0038‡	...	1653	$2.41 \pm 0.10 \pm 0.13$	$5.55 \pm 0.20 \pm 0.27$	155.92	0.68	no/no	$5.38 \pm 0.19 \pm 0.25$	0.90
PSR J1227–4853	J1227.9–4854	2449	$2.40 \pm 0.02 \pm 0.06$	$3.72 \pm 0.11 \pm 0.07$	186.98	–48.90	no/yes	$17.80 \pm 0.53 \pm 0.34$	2.00
PSR J1227–4853†	J1227.9–4854	2059	$2.36 \pm 0.06 \pm 0.09$	$4.57 \pm 0.15 \pm 0.08$	186.98	–48.90	no/yes	$21.85 \pm 0.70 \pm 0.42$	2.00
PSR J1227–4853‡	J1227.9–4854	370	$2.42 \pm 0.03 \pm 0.15$	$1.79 \pm 0.16 \pm 0.17$	186.98	–48.90	no/yes	$8.57 \pm 0.75 \pm 0.82$	2.00
PSR J1431–4715	...	13	...	< 0.45	217.75	–47.25	no/yes	< 1.36	2.42
3FGL J1544.6–1125	J1544.6–1125	407	$2.48 \pm 0.05 \pm 0.11$	$1.43 \pm 0.09 \pm 0.04$	236.17	–11.43	no/no
PSR J1628–3205	J1628.0–3203	372	$2.36 \pm 0.02 \pm 0.04$	$1.01 \pm 0.09 \pm 0.09$	247.02	–32.06	no/yes	$2.87 \pm 0.25 \pm 0.26$	1.54
3FGL J1653.6–0158	J1653.6–0158	2911	$2.24 \pm 0.02 \pm 0.07$	$3.28 \pm 0.12 \pm 0.05$	253.42	–1.98	no/no
PSR J1723–2837	...	35	$2.67 \pm 0.15 \pm 0.17$	$0.83 \pm 0.23 \pm 0.40$	260.75	–28.62	no/no	$0.56 \pm 0.16 \pm 0.15$	0.75
PSR J1816+4510	J1816.5+4512	952	$2.12 \pm 0.04 \pm 0.02$	$0.94 \pm 0.06 \pm 0.04$	274.13	45.20	no/yes	$19.92 \pm 1.22 \pm 0.81$	4.20
PSR J2129–0429	J2129.6–0427	402	$2.22 \pm 0.05 \pm 0.06$	$1.10 \pm 0.08 \pm 0.03$	322.41	–4.46	no/yes	$1.40 \pm 0.10 \pm 0.04$	1.03
PSR J2215+5135	J2215.6+5134	788	$2.08 \pm 0.04 \pm 0.09$	$1.33 \pm 0.09 \pm 0.06$	333.91	51.58	yes/yes	$17.32 \pm 1.12 \pm 0.75$	3.30
PSR J2339–0533	J2339.6–0533	3963	$1.94 \pm 0.01 \pm 0.04$	$5.05 \pm 0.19 \pm 0.53$	354.90	–5.55	no/yes	$7.30 \pm 0.27 \pm 0.77$	1.10
<hr/>									
BW name									
PSR B1957+20	J1959.5+2047	562	$2.40 \pm 0.04 \pm 0.38$	$1.52 \pm 0.02 \pm 0.06$	299.89	20.80	yes/yes	$4.05 \pm 0.33 \pm 0.38$	1.53
PSR J0023+0923	J0023.4+0923	407	$2.27 \pm 0.01 \pm 0.08$	$0.79 \pm 0.07 \pm 0.13$	5.86	9.39	yes/yes	$0.85 \pm 0.07 \pm 0.14$	0.95
PSR J0610–2100	J0610.2–2059	366	$2.28 \pm 0.05 \pm 0.04$	$1.09 \pm 0.08 \pm 0.04$	92.55	–20.99	yes/yes	$41.44 \pm 2.97 \pm 1.65$	5.64
PSR J1124–3653	J1123.9–3653	1041	$2.12 \pm 0.04 \pm 0.07$	$1.28 \pm 0.08 \pm 0.03$	170.99	–36.89	yes/yes	$29.60 \pm 1.88 \pm 0.57$	4.40
PSR J1301+0833	J1301.6+0832	505	$2.25 \pm 0.05 \pm 0.08$	$1.18 \pm 0.08 \pm 0.13$	195.42	8.54	no/yes	$1.17 \pm 0.08 \pm 0.13$	0.91
PSR J1311–3430	J1311.8–3430	9523	$2.21 \pm 0.01 \pm 0.04$	$6.20 \pm 0.13 \pm 0.04$	197.96	–34.50	no/yes	$102.72 \pm 2.13 \pm 0.78$	3.72
PSR J1446–4701	J1446.6–4701	163	$2.08 \pm 0.03 \pm 0.05$	$0.91 \pm 0.08 \pm 0.07$	221.66	–47.03	yes/yes	$4.47 \pm 0.41 \pm 0.35$	2.03
PSR J1544+4937	J1544.0+4938	156	$2.27 \pm 0.09 \pm 0.09$	$0.45 \pm 0.05 \pm 0.02$	236.02	49.65	no/yes	$2.85 \pm 0.31 \pm 0.14$	2.30
PSR J1653–2054	...	1	$1.47 \pm 0.73 \pm 0.16$	< 0.14	253.38	–20.92	no/no	< 0.53	2.64
PSR J1731–1847	...	6	$2.32 \pm 0.20 \pm 0.38$	< 0.55	262.82	–18.79	no/no	< 4.65	4.03
PSR J1745+1017	...	0.00	$2.38 \pm 12.64 \pm 0.32$	< 0.17	266.25	10.28	no/yes	< 0.12	1.36
PSR J1810+1744	J1810.5+1743	1701	$2.35 \pm 0.03 \pm 0.43$	$2.34 \pm 0.09 \pm 0.18$	272.64	17.72	yes/yes	$17.38 \pm 0.69 \pm 1.37$	2.49
PSR J2047+1053	J2047.1+1054	140	$2.34 \pm 0.53 \pm 0.12$	$0.29 \pm 0.03 \pm 0.12$	311.78	10.91	yes/yes	$1.74 \pm 0.20 \pm 0.68$	2.23
PSR J2051–0827	J2051.3–0828	126	$2.21 \pm 0.10 \pm 1.09$	$0.33 \pm 0.05 \pm 0.15$	312.83	–8.48	yes/yes	$0.64 \pm 0.11 \pm 0.16$	1.28
PSR J2214+3000	J2214.6+3000	5380	$2.04 \pm 0.02 \pm 0.05$	$3.16 \pm 0.09 \pm 0.01$	333.66	30.01	yes/yes	$6.58 \pm 0.18 \pm 0.03$	1.32
PSR J2234+0944	J2234.8+0945	720	$2.20 \pm 0.05 \pm 0.10$	$1.14 \pm 0.09 \pm 0.10$	338.71	9.75	no/yes	$1.45 \pm 0.11 \pm 0.13$	1.03
PSR J2241–5236	J2241.6–5237	6424	$2.03 \pm 0.02 \pm 0.07$	$3.27 \pm 0.09 \pm 0.03$	340.42	–52.62	yes/yes	$1.81 \pm 0.05 \pm 0.02$	0.68
PSR J2256–1024	J2256.7–1022	439	$2.02 \pm 0.05 \pm 0.05$	$0.56 \pm 0.05 \pm 0.11$	344.18	–10.38	no/no	$0.55 \pm 0.05 \pm 0.11$	0.91

^aGamma-ray pulsations from J1023+0038 were detected by Archibald et al. (2013); pulsations from J1227–4853 were detected by Johnson et al. (2015).

Table 2: Long-term light curve fit results. Columns indicate the binning, the χ^2 of a constant fit (except for J1023+0038 in the whole time period and before the transition, see Fig. 3, and other cases where only upper limits are obtained) and the number of degrees of freedom, its P -value and σ . The last two columns (jump factor & data points) represent the features of the transitions that our analysis can rule out (see section 3.2 for details). † and ‡ indicate the data period before and after the state transition. Ellipses are used when a value is not available. In the case of J2234+0944 we also present the fittings before (†) and after (‡) the jump visible in Fig. 3. For details, see text.

RB name PSR	Binning (days)	χ^2	dof	P -value	σ	Jump factor	Data points
3FGL J0523.3–2528	66.9	52.6	36	3.7×10^{-2}	2.1	1.74	2
PSR J1023+0038	9.3
PSR J1023+0038†	9.3
PSR J1023+0038‡	9.3	67.0	62	0.3	1.0
PSR J1227–4853	53.5	205.7	44	$\ll 10^{-10}$	9.8
PSR J1227–4853†	53.5	77.1	29	3.1×10^{-6}	4.7
PSR J1227–4853‡	53.5	13.0	14	0.5	0.6	1.87	4
PSR J1431–4715
3FGL J1544.6–1125	214.8	6.6	10	0.8	0.3	1.63	4
PSR J1628–3205	833.8	3.9	2	0.1	1.5	1.47	1
3FGL J1653–0158	36.5	73.3	67	0.3	1.1	1.74	5
PSR J1723–2837	368.0	1.1	1	0.3	1.0	2.18	2
PSR J1816+4510	94.0	23.2	24	0.5	0.7	1.77	4
PSR J2129–0429	311.7	5.4	7	0.6	0.5	1.60	4
PSR J2215+5135	138.6	10.1	17	0.9	0.1	1.68	5
PSR J2339–0533	24.5	128.0	96	1.6×10^{-2}	2.4	1.91	2
BW name							
PSR B1957+20	192.0	9.8	12	0.6	0.5	1.60	4
PSR J0023+0923	156.0	7.5	14	0.9	0.1	1.81	5
PSR J0610–2100	171.1	7.0	14	0.9	0.1	1.80	5
PSR J1124–3653	104.4	19.3	23	0.7	0.4	1.72	5
PSR J1301+0833	126.4	31.7	17	1.7×10^{-2}	2.4	1.85	1
PSR J1311–3430	11.8	183.3	203	0.8	0.2	1.76	11
PSR J1446–4701	506.4	26.3	4	2.7×10^{-5}	4.2	2.09	...
PSR J1544+4937	370.2	2.5	6	0.9	0.2	1.85	5
PSR J1653–2054
PSR J1731–1847
PSR J1745+1017
PSR J1810+1744	48.7	63.9	48	6.2×10^{-2}	1.9	1.75	3
PSR J2047+1053	445.6	4.4	5	0.5	0.7	1.99	3
PSR J2051–0827	688.6	1.4	3	0.7	0.4	1.79	4
PSR J2214+3000	17.9	116.4	131	0.8	0.2	1.85	9
PSR J2234+0944	106.7	77.8	22	3.7×10^{-8}	5.5	1.82	...
PSR J2234+0944†	106.7	9.5	7	0.2	1.2	1.84	2
PSR J2234+0944‡	106.7	17.4	14	0.2	1.2	1.66	3
PSR J2241–5236	15.2	138.8	153	0.8	0.3	1.90	10
PSR J2256–1024	182.6	11.5	10	0.3	1.0	1.77	3

The *Fermi*-LAT Collaboration acknowledges support from a number of agencies and institutes for both development and the operation of the LAT as well as scientific data analysis. These include NASA and DOE in the United States, CEA/Irfu and IN2P3/CNRS in France, ASI and INFN in Italy, MEXT, KEK, and JAXA in Japan, and the K. A. Wallenberg Foundation, the Swedish Research Council and the National Space Board in Sweden. Additional support from INAF in Italy and CNES in France for science analysis during the operations phase is also gratefully acknowledged.

We acknowledge the support from the grants AYA2015-71042-P, SGR 2014-1073 and the National Natural Science Foundation of China via NSFC-11473027, NSFC-11503078, NSFC-11133002, NSFC-11103020, XTP project XDA 04060604 and the Strategic Priority Research Program “The Emergence of Cosmological Structures” of the Chinese Academy of Sciences, Grant No. XDB09000000, as well as the CERCA Programme of the Generalitat de Catalunya. N.R. is further supported by an NWO Vidi Award. A.P. acknowledge support via an EU Marie Skłodowska-Curie Individual Fellowship under contract No. 660657-TMSP-H2020-MSCA-IF-2014, as well as we all acknowledge fruitful discussion with the international team on “The disk-magnetosphere interaction around transitional millisecond pulsars” at ISSI (International Space Science Institute), Bern. We thank T. J. Johnson and P. S. Ray for comments.

REFERENCES

- Abdo, A. A., Ackermann, M., Ajello, M., et al. 2010a, *A&A*, 524, 75
- Abdo, A. A., Ackermann, M., Ajello, M., et al. 2010b, 2010 *ApJ* 722, 520
- Abdo, A. A., Ajello, M., Allafort, A., et al. 2013, *ApJS*, 208, 17
- Acero, F., Ackermann, M., Ajello, M., et al. 2015, *ApJS*, 218, 23 (3FGL)
- Acero, F., Ackermann, M., Ajello, M., et al. 2016, *ApJS*, 223, 26
- Ackermann, M., Ajello, M., Albert, A., et al. 2012, *ApJS*, 203, 4
- Alpar, M. A., Cheng, A. F., Ruderman, M. A. & Shaham, J. 1982, *Nature*, 300, 728
- Archibald, A. M., Stairs, I. H., Ransom, S. M. et al. 2009 *Science*, 324, 1411

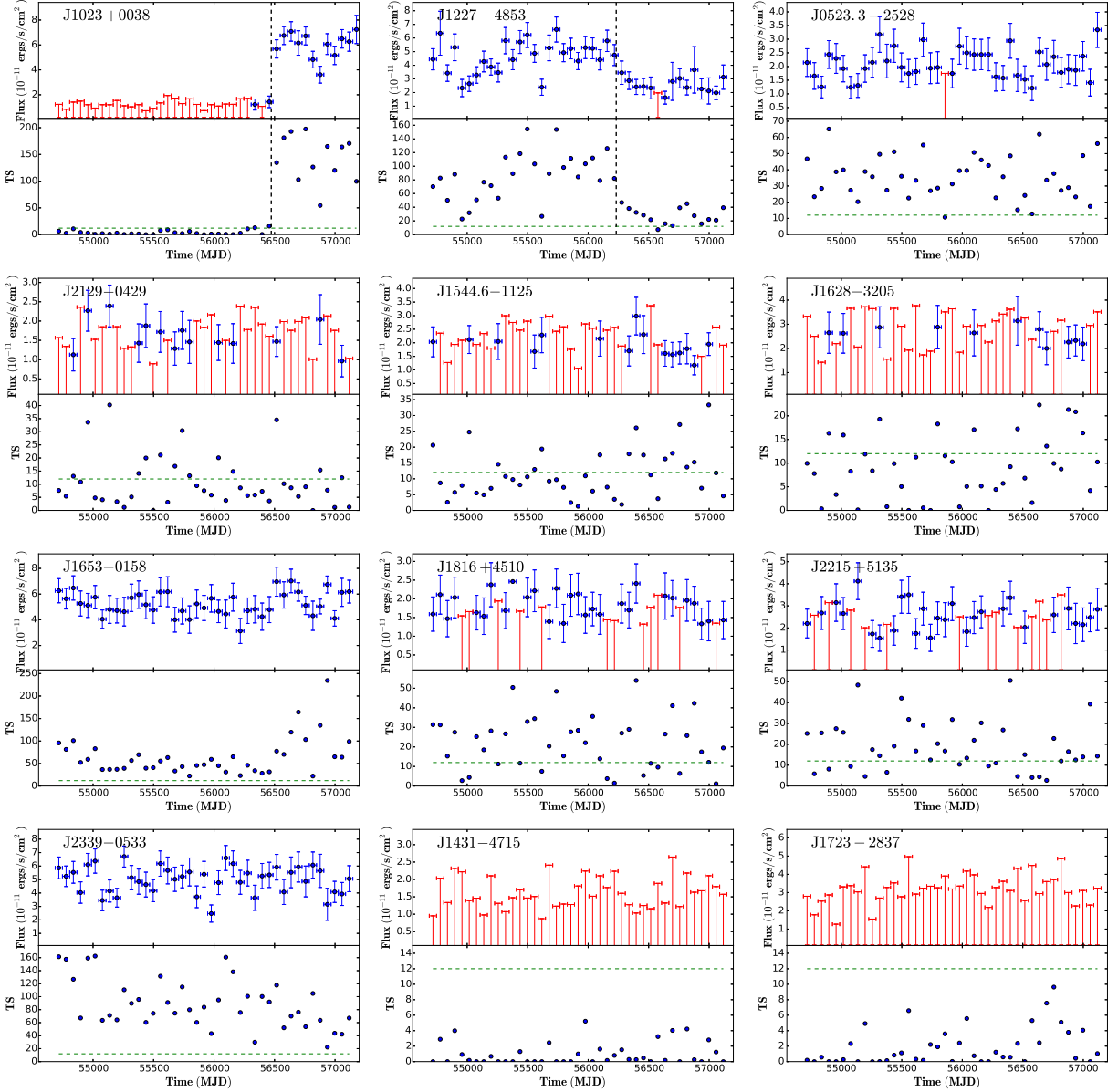


Fig. 1.— First two panels: Long-term light curves of the transitional millisecond pulsars J1023+0038 and J1227–4853. The already known (Stappers et al. 2014; Bassa et al. 2014) state transitions are indicated with dotted vertical lines. The red lines show the flux upper limits. The dotted horizontal green line indicates TS=12. Subsequent panels: Long-term light curves of RBs and BWs studied (other than J1023+0038 and J1227–4853). The color coding remains the same. The time binning is 60 days in all cases.

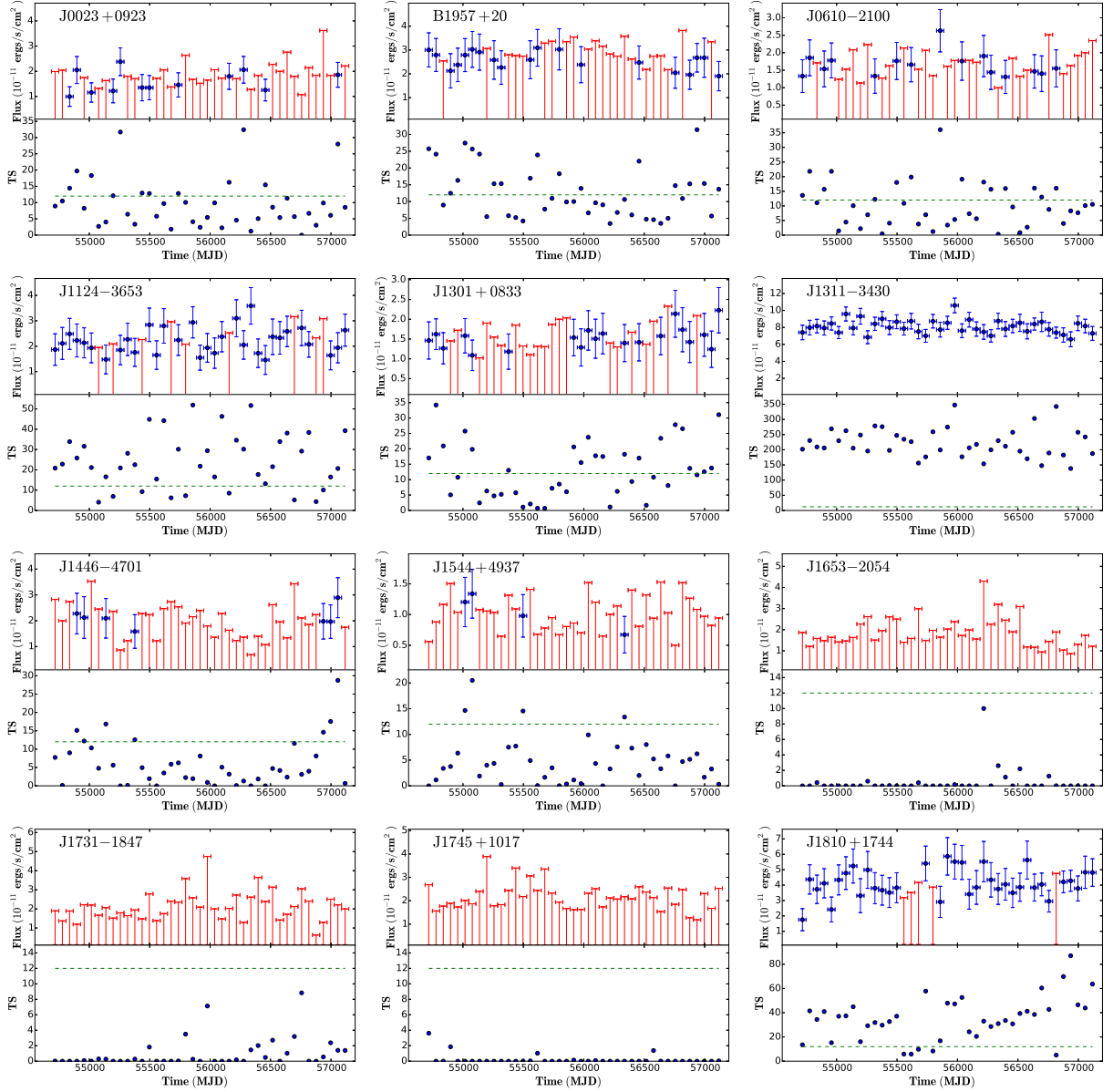


Fig. 1.— *Continued*

Archibald, A. M., Kaspi, V. M., Hessels, J. W. T. et al. 2013 arXiv:1311.5161

Archibald, A. M., Bogdanov, S., Patruno, A. et al. 2015, ApJ 807, 62

Arumugasamy, P., Pavlov, G. G.; Garmire, G. P. 2015, ApJ, 814, 90

Bassa, C. G., Patruno, A., Hessels, J. W. T., et al. 2014, MNRAS, 441, 1825

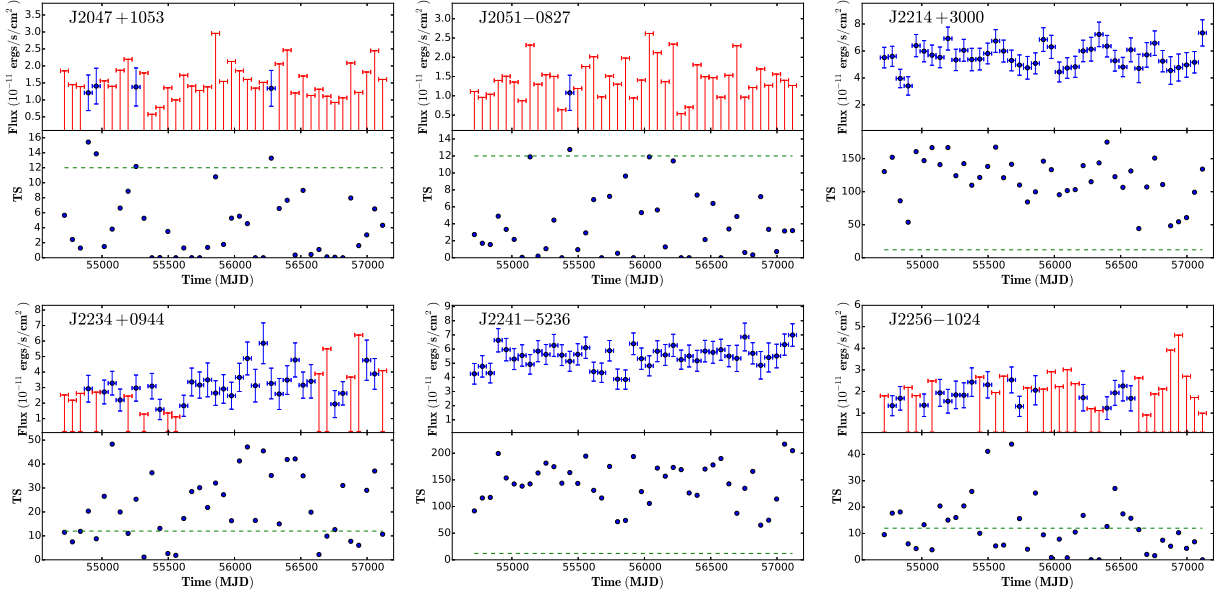


Fig. 1.— *Continued*

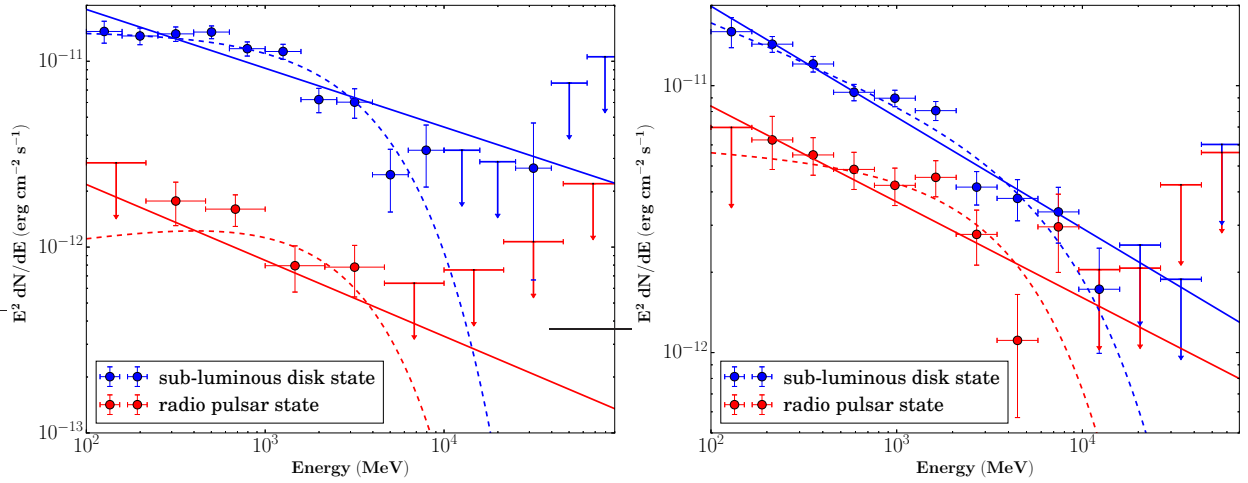


Fig. 2.— *Fermi*-LAT spectra of J1023+0038 (left) and J1227–4853 (right), in radio pulsar state (red) and sub-luminous disk state (blue). The corresponding *gtlike*-fitted models are shown with solid lines (for a power-law) and dotted lines (for a power law with exponential cutoff).

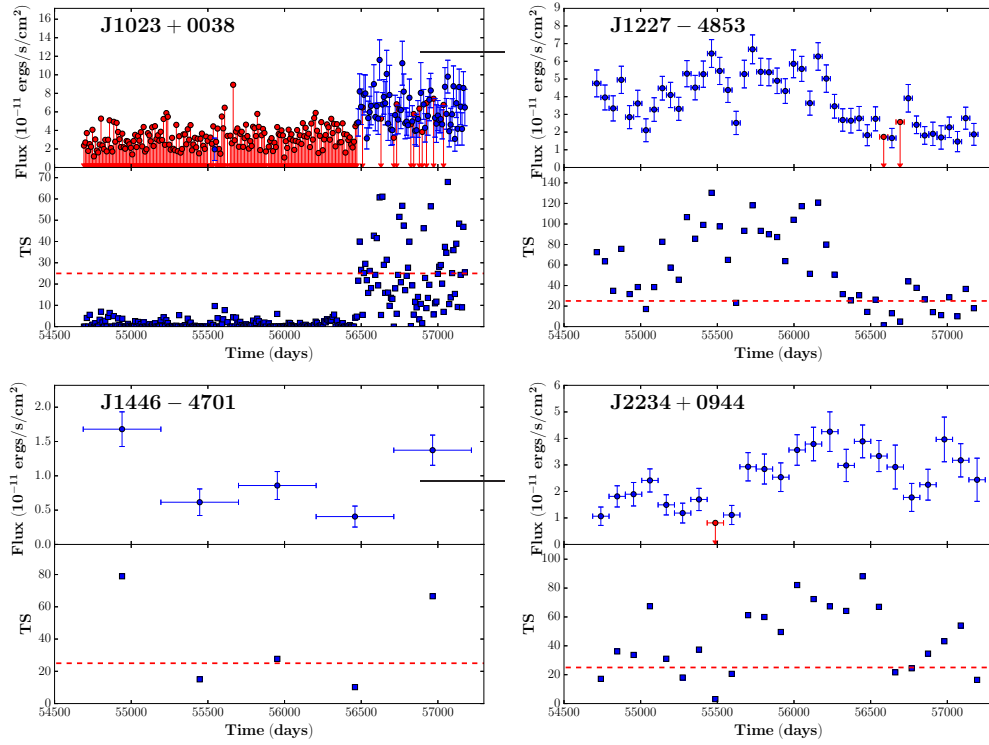


Fig. 3.— Long-term light curves of J1023+0038, J1227-4853, J1446-4701 and J2234+0944, for time bins defined case-by-case via simulations. The dotted horizontal line indicates TS=25. See text for details.

- Bogdanov S. & Halpern J. 2015, ApJL, 803, 27
- Bogdanov S. 2015, ApJ 806, 148,
- Bogdanov S. 2016, 2016, ApJ, 826, 28
- Campana, S., Coti Zelati, F., Papitto, A., et al. 2016, A&A, 594, 31
- Chen H., Chen X., Tauris T., & Han. Z. 2013, ApJ 775, 27
- Cordes, J. M.& Lazio, T. J. W., 2002, arXiv:astro-ph/0207156
- D’Amico, N., Lyne, A. G., Manchester, R. N., Possenti, A., Camilo, F., 2001, ApJL, 548, 171
- de Martino, D., Falanga, M., Bonnet-Bidaud, J.-M. et al. 2010 A&A 515, 25
- de Martino, D., Belloni, T., Falanga, M. et al. 2013, A&A 550, 89
- de Martino, D., Papitto, A., Belloni, T. et al. 2015, MNRAS 454, 2190
- Fruchter, A. S., Stinebring, D. R., Taylor, J. H. 1988, Nature, 333, 237
- Guillemot, L.& Tauris, T. M., 2014, MNRAS, 439, 2033
- Helene, O., 1983, NIMPR, 212, 319
- Manchester, R. N., Hobbs, G. B., Teoh, A., Hobbs, M., 2005, AJ, 129, 1993
- Mattox, J. R., Bertsch, D. L., Chiang, J. et al, 1996, ApJ 461,396
- Ng, C. W., Takata J., and Cheng K. S. 2016, ApJ, 825, 18
- Johnson, T. J., Ray, P. S., Roy, J. et al. 2015, ApJ 806, 91
- Keith, M. J., Johnston, S., Bailes, M. et al. 2012, MNRAS, 419, 1752
- Papitto, A., Ferrigno, C., Bozzo, E. et al. 2013 Nature 501, 517
- Papitto, A., Li, J., & Torres, D. F. 2014, MNRAS 438, 2105
- Papitto, A. & Torres D. F. 2015, ApJ 807, 33
- Papitto, A., de Martino, D., Belloni, T. M. et al. 2015, MNRAS Letters 449, 26
- Papitto A., Torres D. F., Rea N., & Tauris, T. M. 2014, A&A 566, A64

Ray, P., Abdo, A. A., Parent, D. et al. 2012, 2011 Fermi Symposium, Roma, May. 9-12, eConf C110509 [astro-ph/1205.3089]

Roy, J., Ray, P. S., Bhattacharyya, B. et al. 2015, ApJ Letters 800, 12

Stappers, B. W., Archibald, A. M., Hessels, J. W. T. et al., 2014, ApJ, 790, 39

Tam, P. H. T., Hui, C. Y., Huang, R. H. H. et al. 2010, ApJL, 724, 207

Takata, J., Li, K. L., Leung, Gene C. K. et al. 2014, ApJ, 785, 131

Xing, Y & Wang, Z. X., 2015, ApJ, 806, 1